

# Recursive Mode Matching Method for Multiple Waveguide Junction Modeling

Olivier P. Franz and Weng Cho Chew, *Fellow, IEEE*

**Abstract**—The mode matching method is applied to different waveguide geometries, and a recursive scheme is defined to use the appropriate number of modes in each section of the waveguide. Numerical simulations for different types of applications are given and show very good results.

## I. INTRODUCTION

A GENERAL algorithm has been developed to solve the multiple waveguide junction problem for any arbitrarily shaped hollow waveguide, using the mode matching method in a symbolic matrix formulation. This method is very popular and has already been used in [1], [5], or [6]. Other methods are known for solving the waveguide discontinuity problem: the multimode network representation [2], the finite element method [3], the scattering matrix representation [4], or the recurrence modal analysis [8].

The mode matching method requires that the electric and magnetic fields inside a waveguide be expressed in terms of an infinite sum of its eigenmodes. After having derived such expressions in each waveguide, one applies the boundary conditions at the junction of two different waveguides to match the fields. Hence, one can derive two matrix equations where the reflection and transmission operators are the unknowns, and then solve for them. In the case of a multiple waveguide junction problem, these operators will be derived at each junction, and general operators will be defined for the entire structure.

The problem of the accuracy in the results is mainly due to the order of truncation of the infinite expansion needed for the fields. We define a condition on the number of modes in each section of the waveguide that gives good precision in the recursive process, whose accurate results are shown using numerical simulations.

## II. THE MODE MATCHING METHOD THEORY

We present the basic formulations of the mode matching method in the general case of an arbitrarily shaped hollow waveguide. We will first recall the expressions obtained in the case of a single junction, as they can be found in [9], and then derive from the equations the expressions of the complete structure's reflection and transmission operators for a double junction and multiple waveguide junctions.

Manuscript received February 21, 1995; revised October 2, 1995.

The authors are with the Electromagnetics Laboratory, Department of Electrical and Computer Engineering, University of Illinois, Urbana, IL 61801 USA.

Publisher Item Identifier S 0018-9480(96)00475-9.

### A. Single Waveguide Junction

The fields have to be expanded in terms of the eigenmodes of the waveguide. For the  $z$ -component, they can be written as

$$H_z = \sum_i H_i \psi_{hi}(r_s) e^{ik_{hi}z} \quad (\text{for TE modes}) \quad (1)$$

$$E_z = \sum_i E_i \psi_{ei}(r_s) e^{ik_{ei}z} \quad (\text{for TM modes}) \quad (2)$$

where  $\psi_{hi}(\mathbf{r}_s)$  and  $\psi_{ei}(\mathbf{r}_s)$  are the solutions to the wave equation  $(\nabla_s^2 + k^2 - k_{iz}^2)\psi_i(\mathbf{r}_s) = 0$  in two dimensions, with Neumann and Dirichlet boundary conditions, respectively. Once the  $z$ -components of the eigenvectors are known, the transverse components can be easily derived using Maxwell's equations

$$E_s = \sum_i \left[ \frac{E_i}{k_{eis}^2} ik_{eiz} \nabla_s \psi_{ei}(r_s) e^{ik_{eiz}z} - \frac{i\omega\mu H_i}{k_{his}^2} \hat{z} \times \nabla_s \psi_{hi}(r_s) e^{ik_{his}z} \right] \quad (3)$$

$$H_s = \sum_i \left[ \frac{i\omega\epsilon E_i}{k_{eis}^2} \hat{z} \times \nabla_s \psi_{ei}(r_s) e^{ik_{eiz}z} + \frac{H_i}{k_{his}^2} ik_{his} \nabla_s \psi_{hi}(r_s) e^{ik_{his}z} \right] \quad (4)$$

where  $k_{eis}^2 = k^2 - k_{eiz}^2$  and  $k_{his}^2 = k^2 - k_{hiz}^2$ .

As shown in [9], after rearranging the terms into two groups, one for the TE and one for the TM modes, (3) and (4) become

$$E_s = \Psi^t(r_s) \cdot e^{iKz} \cdot e \quad (5)$$

$$\hat{z} \times H_s = -\Psi^t(r_s) \cdot G \cdot e^{iKz} \cdot e. \quad (6)$$

Then, we define

$$D_i = \langle \Psi_i, \Psi_i^t \rangle = \int_{S_a} dS \Psi_i(r_s) \cdot \Psi_i^t(r_s) \quad (7)$$

$$L_{ia} = \langle \Psi_i, \Psi_a^t \rangle = \int_{S_a} dS \Psi_i(r_s) \cdot \Psi_a^t(r_s) \quad (8)$$

so that we can derive from the boundary conditions a set of expressions for the operators  $R$  and  $T$  (see [10])

$$R = D_1^{-1} : L_{1a} \cdot (L_{1a}^t : G_1 : D_1^{-1} : L_{1a} + L_{2a}^t : G_2 : D_2^{-1} : L_{2a})^{-1} 2L_{1a}^t : G_1 - I \quad (9)$$

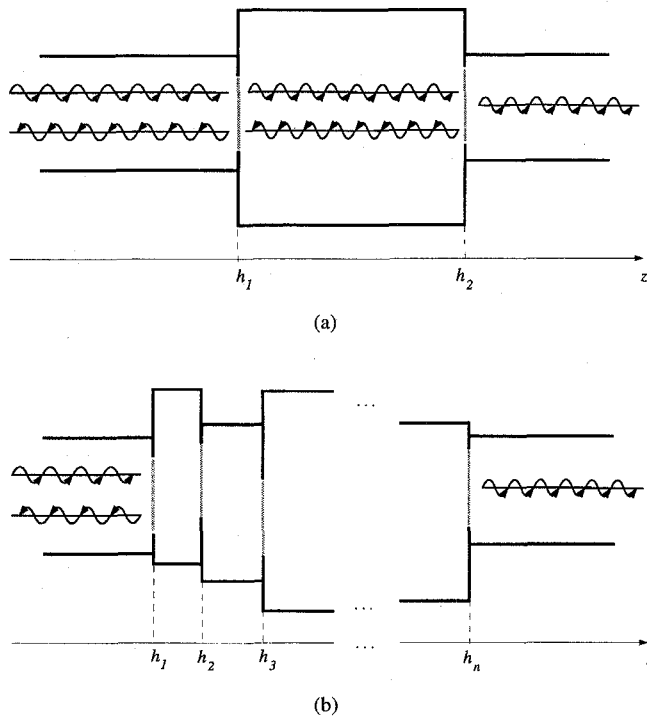


Fig. 1. (a) Double junction and (b) multiple junction.

and

$$T = D_2^{-1} : L_{2a} \cdot (L_{1a}^t : G_1 : D_1^{-1} : L_{1a} + L_{2a}^t : G_2 : D_2^{-1} : L_{2a})^{-1} 2L_{1a}^t : G_1. \quad (10)$$

### B. Double Waveguide Junction

In this case, the electric field in the first waveguide can be written with a generalized reflection operator, as those defined in [10] for layered media,  $\tilde{R}_{12}$

$$E_{1s} = \Psi_1^t(r_s) \cdot (e^{iK_1 z} + e^{-iK_1 z} \cdot \tilde{R}_{12}) \cdot e. \quad (11)$$

In the second waveguide, as shown in Fig. 1(a), we will write the solution as a superposition of waves travelling in two directions

$$E_{2s} = \Psi_2^t(r_2) \cdot (e^{iK_2 z} \cdot A_2 + e^{-iK_2 z} \cdot B_2). \quad (12)$$

In the third waveguide, an expression similar to the one derived in (15) can be written

$$E_{3s} = \Psi_3^t(r_s) \cdot e^{iK_3 z} \cdot A_3. \quad (13)$$

All of the coefficients,  $A_2$ ,  $B_2$ , and  $A_3$ , can be found by again applying matching conditions with physical insight [10]. They finally lead to the expression of the generalized reflection and transmission coefficients

$$\tilde{R}_{12} = R_{12} + T_{21} \cdot e^{iK_2(h_2-h_1)} \cdot R_{23} \cdot e^{iK_2(h_2-h_1)} \cdot (I - R_{21} \cdot e^{iK_2(h_2-h_1)} \cdot R_{23} \cdot e^{iK_2(h_2-h_1)})^{-1} \cdot T_{12}. \quad (14)$$

These intermediate results are now applied to the multiple waveguide junction problem.

### C. Multiple Waveguide Junction

By analogy with the double waveguide junction problem, the following expressions for the field in waveguide  $j$ , the generalized reflection operator  $\tilde{R}_{j,j+1}$ , and the amplitude  $A_j$ , can be derived in the case of an  $N$  waveguide junction, as shown in Fig. 1(b)

$$E_{js} = \Psi_j^t(r_s) \cdot (e^{iK_j z} + e^{-iK_j(z-h_j)} \cdot \tilde{R}_{j,j+1} \cdot e^{iK_j h_j}) \cdot A_j \quad (15)$$

$$\begin{aligned} \tilde{R}_{j,j+1} = & R_{j,j+1} + T_{j+1,j} \cdot e^{iK_{j+1}(h_{j+1}-h_j)} \\ & \cdot \tilde{R}_{j+1,j+2} \cdot e^{iK_{j+1}(h_{j+1}-h_j)} \\ & \cdot [I - R_{j,j+1} \cdot e^{iK_{j+1}(h_{j+1}-h_j)} \\ & \cdot \tilde{R}_{j+1,j+2} \cdot e^{iK_{j+1}(h_{j+1}-h_j)}]^{-1} \cdot T_{j,j+1} \end{aligned} \quad (16)$$

and

$$\begin{aligned} A_j = & e^{-iK_j h_{j-1}} \cdot (I - R_{j,j-1} \cdot e^{iK_j(h_j-h_{j-1})} \\ & \cdot \tilde{R}_{j,j+1} \cdot e^{iK_j(h_j-h_{j-1})})^{-1} \\ & \cdot T_{j-1,j} \cdot e^{iK_{j-1} h_{j-1}} \cdot A_{j-1} \end{aligned} \quad (17)$$

or, in a more compact form

$$A_j = S_{j-1,j} \cdot A_{j-1}. \quad (18)$$

With these recursive equations, an algorithm which finds the expression of the field everywhere in the waveguide, and the generalized reflection and transmission operators of any structure composed of arbitrarily shaped waveguides, can be implemented. The reflection and transmission operators of the entire set of discontinuities are defined by the following

$$\tilde{R} = \tilde{R}_{1,2} \quad (19)$$

$$\tilde{T} = T_{N-1,N} \cdot S_{N-2,N-1} \cdots S_{1,2}. \quad (20)$$

The expressions of the reflection and the transmission operators have been derived, with no loss of generality; we just considered a series of circular hollow waveguides. The only problem is that the mode matching method requires in theory an infinite series expansion of the fields. In the numerical implementation, we will have to truncate the expansion of the fields; the choice of the number of modes is very difficult. One solution is to determine numerically, by trial-and-error, the minimum number of modes needed in the three expansions ( $\Psi_1$ ,  $\Psi_2$ , and  $\Psi_a$ ). But there are also methods in the literature that give conditions on these numbers. Therefore, a recursive scheme can be deduced to find them; in fact, it would have been impossible to do it numerically in the case of a multiple waveguide junction.

### III. OPTIMIZATION OF THE TRUNCATION PROBLEM

The main problem of the mode matching method is the determination of the number of modes necessary to obtain an accurate result. It can be shown by integral equation formulation [10], if  $N$  is large enough, that the following relations have to be satisfied

$$\frac{P_1}{d_1} > \frac{N}{d_a}, \quad \frac{P_2}{d_2} > \frac{N}{d_a}, \quad \frac{P_1}{d_1} \simeq \frac{P_2}{d_2} \quad (21)$$

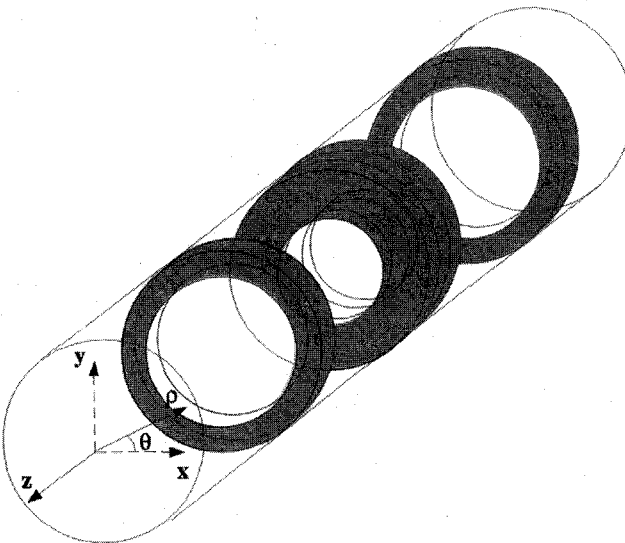


Fig. 2. Geometry of the circular waveguide stopband filter.

where  $P_i$  is the number of modes in region  $i$ ,  $N$  is the number of modes on the diaphragm,  $d_i$  is the size of waveguide  $i$ , and  $a_d$  is the size of the diaphragm.

In the case of a rectangular waveguide, we defined  $P_{x,i}$ ,  $P_{y,i}$ ,  $N_x$  and  $N_y$  as the number of modes in the  $x$ - or  $y$ -directions. In each direction, (21) needs to be satisfied. Our numerical results show that for  $N \simeq 24$ , the values obtained for the  $TE_{10}$  reflection coefficient are very good. This represents approximately four modes in each direction. For multiple waveguide junctions, we use the following equations to find the number of required modes. In the case of a rectangular waveguide, in the  $x$ - and  $y$ -directions

$$\frac{P_{x,1}}{a_1} = \frac{P_{x,2}}{a_2} = \frac{N_x}{a_d}, \quad \frac{P_{y,1}}{b_1} = \frac{P_{y,2}}{b_2} = \frac{N_y}{b_d}. \quad (22)$$

In the case of a circular waveguide, in the  $\rho$ - and  $\phi$ -directions,

$$\frac{P_{\rho,1}}{a_1} = \frac{P_{\rho,2}}{a_2} = \frac{N_{\rho}}{a_d}, \quad \frac{P_{\phi,1}}{a_1} = \frac{P_{\phi,2}}{a_2} = \frac{N_{\phi}}{a_d}. \quad (23)$$

Equations (22) and (23) are similar to (21), but are applied to each dimension of the waveguide section; because these dimensions ( $x$  and  $y$  for the rectangular case,  $\rho$  and  $\phi$  in the circular case) are independent of each other in the basis expansion. The process is repeated for each new junction using the preceding values.

#### IV. NUMERICAL RESULTS

This section shows numerical results in comparison to those found in the literature. We will consider complex geometries with ten or more discontinuities. They show the capability of the waveguide junction modeling theory and its applications.

The circular waveguide filter example has been taken from [5], and our results show very good agreement. The geometry of the structure (see Figs. 2 and 3) is such that the waveguide operates as a filter for a certain range of frequencies, that are only determined by the geometry of the waveguides, as shown on Fig. 4. The case of the corrugated waveguide polarizer has been checked with [6] and [7] and shows good agreement. The

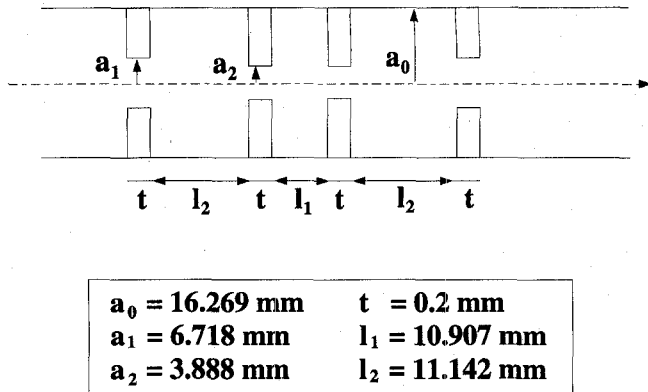


Fig. 3. Numerical lengths of the circular waveguide stopband filters.

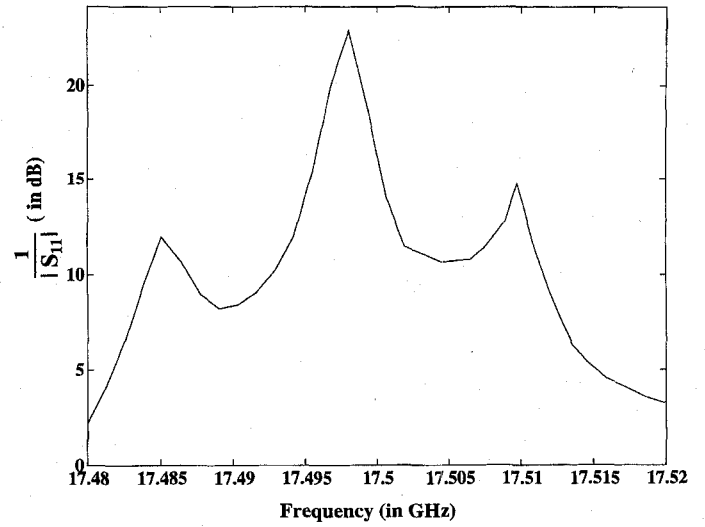


Fig. 4. Return loss of the circular waveguide filter, with its three stopband poles.

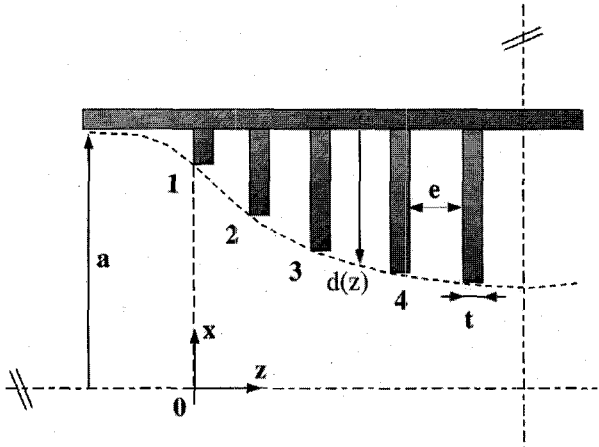


Fig. 5. Geometry of a profiled depth corrugated waveguide polarizer.

symmetric geometry is given in Fig. 5, where  $d(z)$  is known as the profile function and defines the slot depth of the

TABLE I  
(a) CORRUGATED WAVEGUIDE SLOT DEPTHS AND (b) LOW-PASS FILTER LENGTHS

Quantity	Size in mm
$a$	17.997
$b$	17.997
$e$	3.720
$t$	0.942
$d_1$	0.279
$d_2$	0.513
$d_3$	0.746
$d_4$	0.980
$d_5$	1.214
$d_6$	1.447
$d_7$	1.681
$d_8$	1.914

(a)

Quantity	Size in mm
$a$	19.05
$b_1$	19.05
$b_2$	16.62
$b_3$	14.18
$b_4$	11.75
$b_5$	9.32
$b_6$	8.11
$b_7$	21.48
$l_1$	1.94
$l_2$	3.72
$l_3$	4.51

(b)

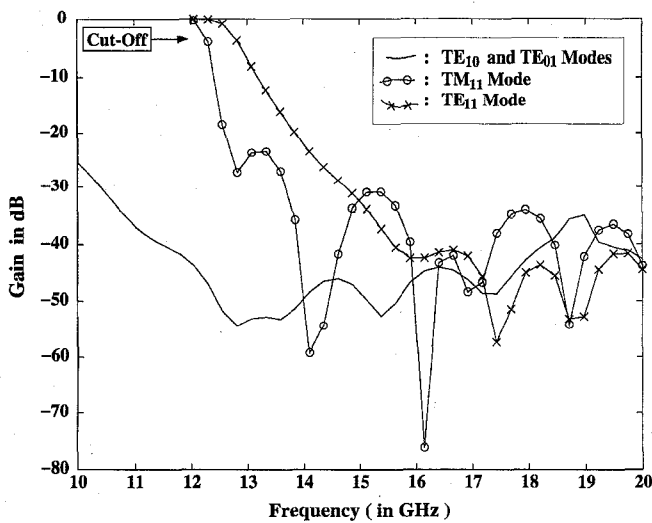


Fig. 6. Gain of different waveguide modes for the corrugated square waveguide polarizer.

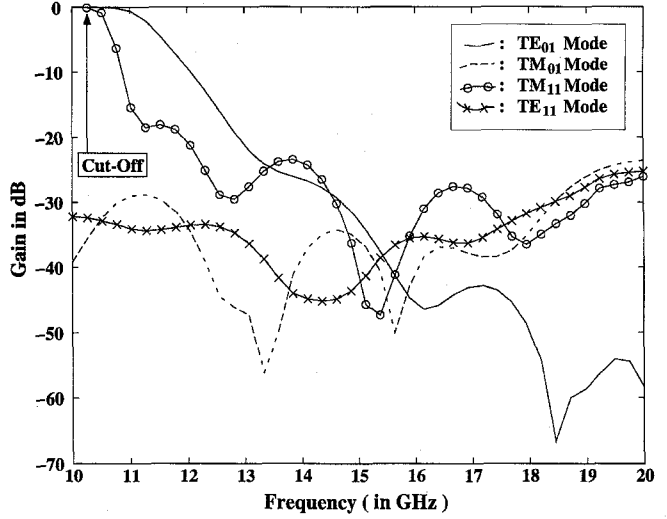


Fig. 8. Gain of different waveguide modes for the corrugated circular waveguide polarizer.

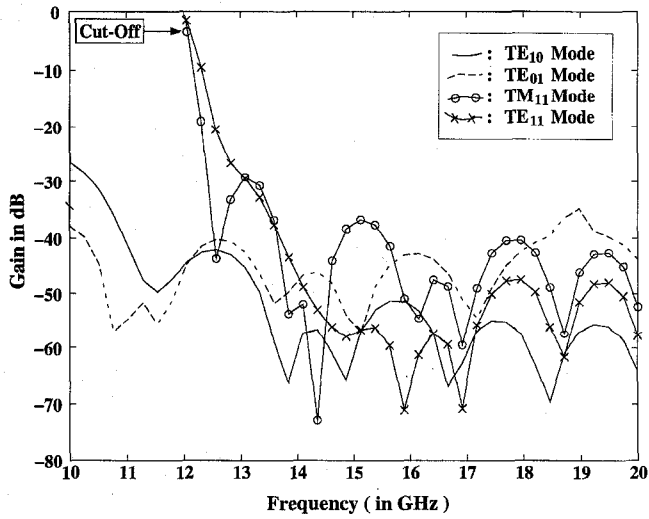


Fig. 7. Gain of different waveguide modes for the corrugated rectangular waveguide polarizer.

discontinuities. The example analyzed here uses a linear profile function, which enables us to obtain the slot depths defined in Table I(a). We consider 30 discontinuities for different

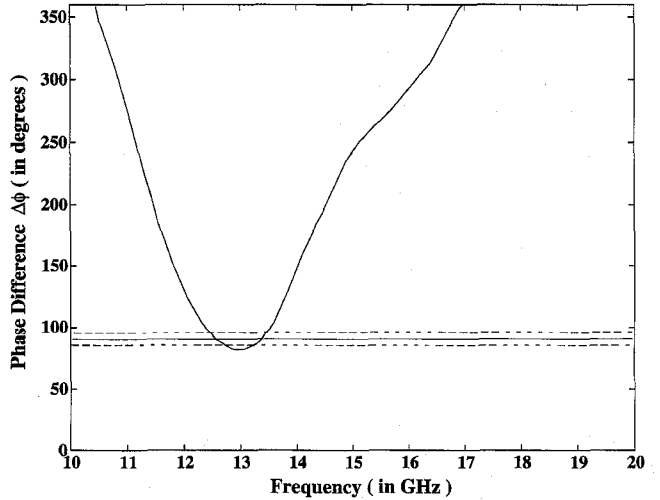


Fig. 9. Difference of phase between the TE01 and TE11 modes for the corrugated circular waveguide polarizer.

dominant modes in three different cases. The first case is for a square waveguide geometry, which means that the geometry is the same in the  $x$ - and  $y$ -directions, and the results are shown

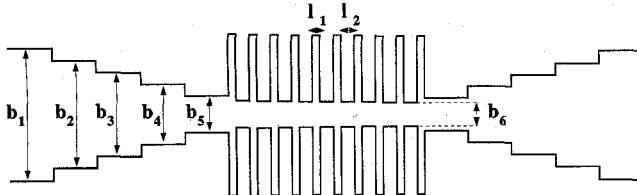


Fig. 10. Geometry of the first low-pass filter.

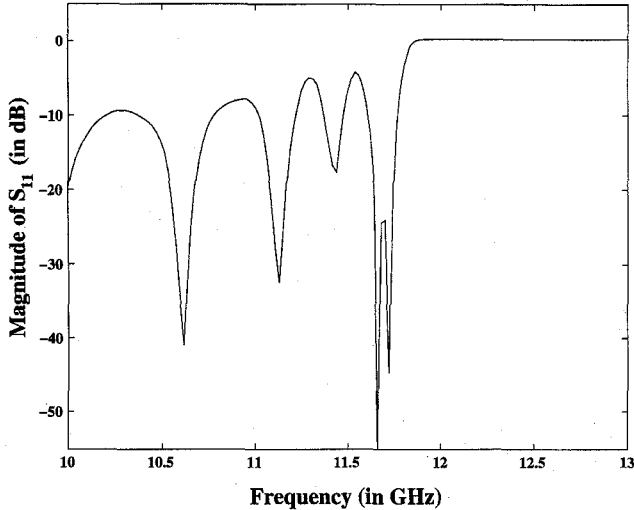
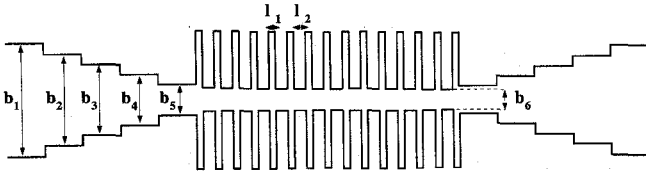
Fig. 11. Magnitude of  $S_{11}$  for the first low-pass filter.

Fig. 12. Geometry of the second low-pass filter.

on Fig. 6, where the gain is defined by  $G_{dB} = 20 \log R$ . For the results of Fig. 7, we considered a rectangular waveguide geometry, which means that in the  $y$ -direction, the size of the waveguide is constant. Finally we used a circular geometry, whose results are shown in Fig. 8. One of the properties of this kind of waveguide structure is that the differential phase shift  $\Delta\phi$  between two similar modes ( $TE_{01}$  and  $TE_{11}$  for instance) is continuous as a function of the frequency as shown on Fig. 9, where the horizontal lines show the  $90^\circ$  ( $\pm 2^\circ$ ) phase shift area.

Three low-pass filters are finally considered and show good agreement with [1]. The first waveguide filter considered is rectangular. Its geometry is given in Fig. 10. The example analyzed here is an array of capacitive step that becomes a low-pass filter device. The structure has 28 discontinuities; their lengths are presented in Table I(b). From Fig. 11, we can see that the structure is acting as a low-pass filter for the  $TE_{10}$  mode. Ten new elements are added to the structure, as shown in Fig. 12. The result is given in Fig. 13, where it can be seen that the second structure has a slightly higher cut-off.

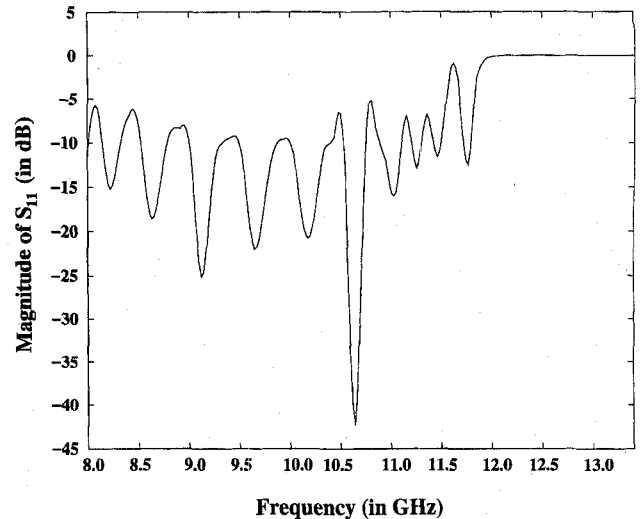
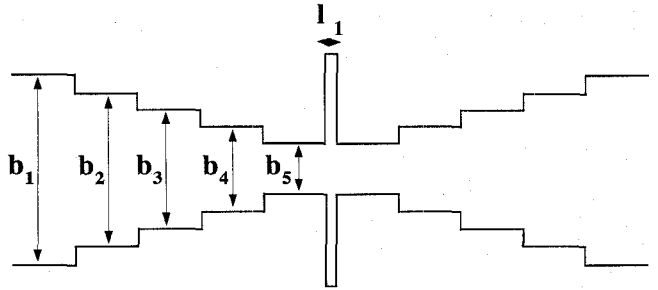
Fig. 13. Magnitude of  $S_{11}$  for the second low-pass filter.

Fig. 14. Geometry of the third low-pass filter.

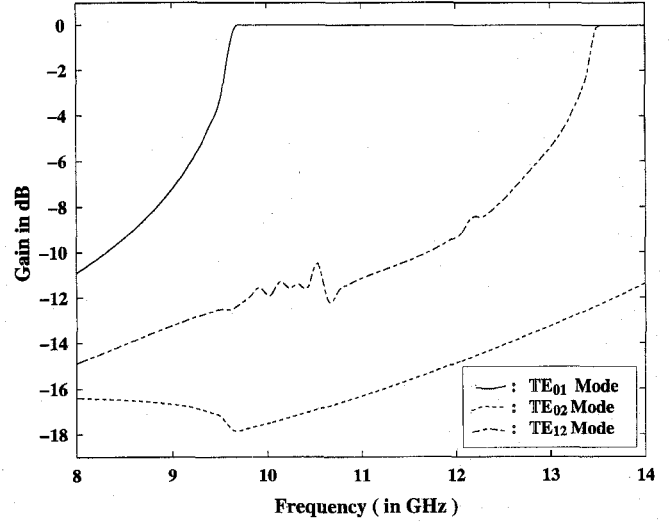


Fig. 15. Gain of some TE modes of the third low-pass filter.

frequency. Finally, the simpler structure of Fig. 14, with circular waveguide elements, gives the results shown in Figs. 15 and 16. We also show the phase of the reflection coefficient of some modes in Fig. 17. On the range of frequency [8.0 GHz, 13.0 GHz], the structure behaves as a phase shifter for most of the modes.

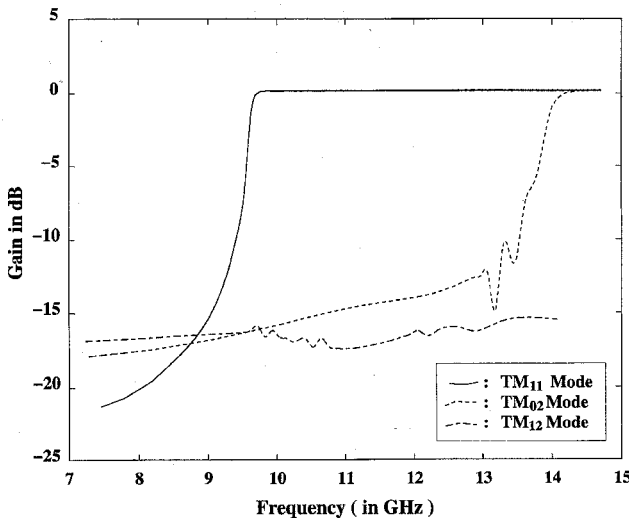


Fig. 16. Gain of some TM modes of the third low-pass filter.

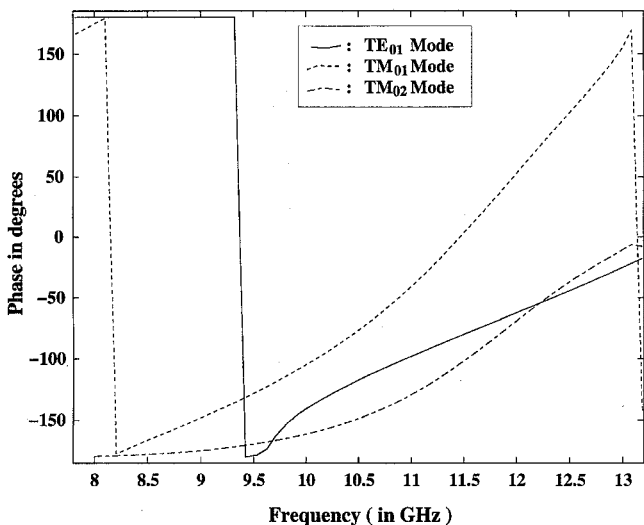


Fig. 17. Phase of some modes of the third low-pass filter.

## V. CONCLUSION

This very powerful method of multiple waveguide junction analysis can be very accurate. The number of unknowns needed (the number of modes) is not too large ( $N \approx 24$  for the rectangular case,  $N \approx 30$  for the circular case). The complexity of the algorithm is then  $O(MN^3)$ , where  $M$  is the number of discontinuities. For each iteration, we have to compute four dense reflection and transmission matrices, which require one matrix inversion and four multiplications. We are presently working on the improvement of the storage and the computation of the matrices, and expect to reduce the complexity to  $O(MN^2)$ .

## REFERENCES

- [1] J. Bornemann and R. Vahldieck, "Characterization of a class of waveguide discontinuities using a modified  $TE_{mn}^x$  mode approach," *IEEE Trans. Microwave Theory Tech.*, vol. 38, no. 12, pp. 1816-1822, Dec. 1990.
- [2] M. Guglielmi and G. Gheri, "Rigorous multimode network representation of capacitive steps," *IEEE Transactions on Microwave Theory and*

- Techniques*, vol. 42, no. 4, pp. 622-628, Apr. 1994.
- [3] G. M. Wilkins, J.-F. Lee and R. Mittra, "Numerical modeling of axisymmetric coaxial waveguide discontinuities," *IEEE Transactions on Microwave Theory and Techniques*, vol. 39, no. 8, pp. 1323-1328, Aug. 1991.
- [4] A. S. Omar and K. Schunemann, "Transmission matrix representation of finline discontinuities," *IEEE Transactions on Microwave Theory and Techniques*, vol. MTT-33, no. 9, pp. 765-770, Sept. 1985.
- [5] U. Papziner and F. Arndt, "Field theoretical computer-aided design of rectangular and circular iris coupled rectangular or circular waveguide cavity filters," *IEEE Transactions on Microwave Theory and Techniques*, vol. 41, no. 3, pp. 462-471, Mar. 1993.
- [6] U. Tucholke and F. Arndt, "Field theory design of square waveguide iris polarizer," *IEEE Transactions on Microwave Theory and Techniques*, vol. MTT-34, no. 1, pp. 156-160, Jan. 1986.
- [7] G. L. James, "Analysis and design of  $TE_{11}$ -to- $HE_{11}$  corrugated cylindrical waveguide mode converters," *IEEE Transactions on Microwave Theory and Techniques*, vol. 29, no. 10, pp. 1059-1066, Oct. 1981.
- [8] G. A. Gesell and I. R. Ceric, "Recurrence modal analysis for multiple waveguide discontinuities and its application to circular structures," *IEEE Transactions on Microwave Theory and Techniques*, vol. 41, no. 3, pp. 484-490, Mar. 1993.
- [9] W. C. Chew, K. H. Lin, J. Friedrich and C. H. Chan, "Reflection and transmission operators for general discontinuities in waveguides," *J. Electromagn. Waves Appl.*, vol. 5, no. 8, pp. 819-834, 1991.
- [10] W. C. Chew, *Waves and Fields in Inhomogeneous Media*. New York: Van Nostrand Reinhold, 1990.

**Olivier P. Franz** was born in Paris, France, on February 13, 1972. He received the Diplome d'Ingenieur Supelec (France) in July 1994, and the M.S. degree in electrical and computer engineering from the University of Illinois at Urbana-Champaign in 1994. He is currently a Ph.D. student at the University of Illinois.



His research interests are 3-D microwave imaging and inverse scattering.

Mr. Franz is a member of the National Confederation of French Engineers and Scientists (CNISF) and the publicity officer of the Illinois Alpha chapter of Tau Beta Pi.

**Weng Cho Chew** (S'79-M'80-SM'86-F'93) was born on June 9, 1953 in Malaysia. He received the B.S. degree in 1976, both the M.S. and engineer's degrees in 1978, and the Ph.D. degree in 1980, all in electrical engineering from the Massachusetts Institute of Technology, Cambridge.

From 1981 to 1985, he was with Schlumberger-Doll Research in Ridgefield, Connecticut. While he was there, he was a Program Leader and later a Department Manager. From 1985 to 1990, he was an Associate Professor with the University of Illinois.

He currently is a Professor there and teaches graduate courses in waves and fields in inhomogeneous media, and theory of microwave and optical waveguides and supervises a graduate research program. His name is often listed in the List of Excellent Instructors on campus. His recent research interest has been in the area of wave propagation, scattering, inverse scattering, and fast algorithms related to scattering, inhomogeneous media for geophysical subsurface sensing and nondestructive testing applications. Previously, he has also analyzed electrochemical effects and dielectric properties of composite materials, microwave and optical waveguides, and microstrip antennas. He has authored a book, *Waves and Fields in Inhomogeneous Media*, published over 110 scientific journal articles and presented over 130 conference papers.

Dr. Chew is a member of Eta Kappa Nu, Tau Beta Pi, URSI Commissions B and F, and an active member with the Society of Exploration Geophysics. He is an IEEE Fellow and was an NSF Presidential Young Investigator for 1986. He was also an AdCom member and is presently an associate editor of the *TRANSACTIONS ON IEEE GEOSCIENCE AND REMOTE SENSING*. He was also an associate editor with the *International Journal of Imaging Systems and Technology*, and has been a Guest Editor of *Radio Science* and *International Journal of Imaging Systems and Technology*. From 1989 to 1993, he was the Associate Director the Advanced Construction Technology Center at the University of Illinois. Presently, he is the Director of the Center for Computational Electromagnetics and the Electromagnetics Laboratory at the same university.

